

Numerical Heat Transfer, Part A: Applications

An International Journal of Computation and Methodology

ISSN: (Print) (Online) Journal homepage: www.tandfonline.com/journals/unht20

Enhancing thermal management in channels with sinusoidal elastic obstacles and pulsating nano-jet impingement: A new model

Momen S.M. Saleh, Ali J. Chamkha & Yousra Bouterfa

To cite this article: Momen S.M. Saleh, Ali J. Chamkha & Yousra Bouterfa (21 Dec 2023): Enhancing thermal management in channels with sinusoidal elastic obstacles and pulsating nano-jet impingement: A new model, Numerical Heat Transfer, Part A: Applications, DOI: [10.1080/10407782.2023.2294048](https://doi.org/10.1080/10407782.2023.2294048)

To link to this article: <https://doi.org/10.1080/10407782.2023.2294048>



Published online: 21 Dec 2023.



Submit your article to this journal [↗](#)



Article views: 66



View related articles [↗](#)



View Crossmark data [↗](#)



Enhancing thermal management in channels with sinusoidal elastic obstacles and pulsating nano-jet impingement: A new model

Momen S.M. Saleh^{a,b} , Ali J. Chamkha^c , and Yousra Boutera^d

^aLaboratory of Materials and Energy Engineering, University of Mohamed Khider Biskra, Algeria; ^bResearch Laboratory of Industrial Technologies, University of Tiaret, Algeria; ^cFaculty of Engineering, Kuwait College of Science and Technology, Kuwait; ^dLaboratoire de Génie Mécanique, LGM, Université de Biskra, Algeria

ABSTRACT

This study presents a new model for effective thermal management of a channel with elastic sinusoidal obstacles and pulsating multiple nano-jet impingements. The channel was cooled by alumina Al_2O_3 in various forms (platelets, blades, cylinders, and bricks) and water as a basic fluid. A hybrid nanofluid (multi-wall carbon nanotube- Fe_3O_4) was also used. The governing equations were solved using the finite volume method. Results were recorded for Reynolds numbers ($Re = 350$), Strouhal numbers ($St = 0.01-1$), pulse amplitude ($A = 0.25-1$), and the number of slots ($N_j = 1-13$). The results showed that the cooling efficiency was improved by using pulsating flow by 24.383%. It was also noted that using sinusoidal elastic obstacles improved the heat transfer rate by 8.344%. In addition, the number of slots affected the heat transfer rate, increasing it to 259.983%. The results obtained from this study demonstrate the effectiveness of the proposed design, which incorporates elastic sinusoidal obstacles and pulsating multiple nano-jet impingements, in significantly improving thermal management performance and reliability. These advancements hold great importance in various industrial and consumer applications.

ARTICLE HISTORY

Received 29 June 2023
Revised 12 November 2023
Accepted 5 December 2023

KEYWORDS

Elastic; nano-jet; pulsating; pulse amplitude; sinusoidal obstacles; thermal management

1. Introduction

Many energy items, including electronics and renewable energy systems, need thermal management for reliable operation, since the heat created by these systems degrades their performance and shortens their lifetime. This necessitates the development of efficient refrigeration systems to get rid of the heat being produced, which is now achievable thanks to technical progress. Due to environmental and financial considerations, developing energy-efficient refrigeration systems is now more important than ever. This prompted many researchers to use nanofluid (NF) as cooling fluids for various cavities due to their importance in many applications in studying two types of convection (forced and mixed), which have many advantages in improving the heat transfer rate (HTR) [1]–[14].

Technological progress and the scientific community prompted researchers to prioritize the study of cavity and membrane motion in order to increase heat transfer rates. Scientists continued their investigation, looking at the effects of obstacles and fins inside channels of varying geometric forms. Incorporating obstacles has been demonstrated to increase the heat transfer (HT) rate [15]–[20].

Nomenclature

Cp	Heat capacity specific $J K^{-1}$	μ	Viscosity dynamic Pa. s
H	height m	ν	Viscosity kinematics m^2 /s
L	width m	ρ	Density $Kg m^{-3}$
k	Thermal conductivity $W m^{-1} K^{-1}$	θ	Dimensionless temperature
Nu	Number of Nusselt	α	Diffusivity of heat $m^2 s^{-1}$
p	Pressure $N m^{-2}$		
P	Dimensionless pressure	Indices	
T	Temperature K	f	Fluid
Pr	Number of Prandtl, $\frac{\nu_f}{\nu_f}$	m	Average
Re	Number of Reynolds	NF	Nano fluid
U, V	Velocity component dimensionless	s	Solid
u, v	Velocity components/(m/s)	w	Wall
X, Y	Dimensionless Cartesian coordinates/(m)	HTR	Heat transfer rate
x,y	Coordinates of Cartesians /(m)	CWO	Channel without obstacles
		COF	Channel obstacles fixed
		COS	Channel obstacles sinusoidal
Greek symbols			
ϕ	Volume fraction of nano fluid		
β	Coefficient of volume expansion K^{-1}		

Several aspects of heat transfer with rigid fins are studied, including the inclination angle [21, 22] and length of the fins [23] and fins located within a cavity [24]; however, industrial problems in light of the development created new problems that called on the scientific community to search for the best ways to solve them. Among the proposed methods is the study of the oscillation of the obstacle that contributed to the fluid turbulence, thus inducing flow and increasing the HTR.

An example of this is the study conducted by Raisi et al. [25] to determine the effect of a flexible barrier placed in the center of the air-filled cavity on natural heat transfer, while Zadeh et al. [26] place a flexible baffle inside the air-filled cavity, and according to the results obtained by the two studies, the flexibility of the baffle improves heat transfer. Also performed numerical study of unsteady natural convection in a differentially heated inclined cavity filled with air was performed by Alsabery et al. [27], using a heat-conductive oscillating flexible fin mounted on the bottom adiabatic wall. They conclude that increasing the amplitude of oscillation enhances heat transmission

On the other hand, Ismail et al. [28, 29] analyzed mixed convection within a cavity, placing a flexible fin on the bottom wall. They found that the flexible fin resulted in a higher heat transfer rate than a rigid fin. Galambaz et al. [29] studied an oscillating fin at the hot wall of a cavity and found that the rate of heat transfer increased with the presence of the oscillating fin and with an increase in its amplitude. Selimefendigil et al. [30] studied fluid flow and heat transfer in a square cavity filled with a nanocopper-water mixture, which was moved by a vertical cap with a flexible fin attached to its upper wall, under the action of an oblique magnetic field, where the results showed that HTR is directly related to the flexibility of the fin. Jamesahar et al. [31] studied the effect of oscillating fins on the heat transfer rate and flow characteristics of a nanofluid inside a square container. The fins were attached to the hot wall and oscillated with the same frequencies and amplitudes. The results showed that the HTR increased due to the fin oscillations.

On the other hand, the high heat fluxes produced by many applications, from nuclear reactors to electronic chips, are removed by various methods and techniques. The new methods used and developed in heat dissipation are known as nano-jet impingement cooling, where it is a rather complex cooling process. However, the high-velocity nanofluid jet creates a thin boundary layer between the fluid and the heated surface, which promotes efficient heat transfer. In their study, Tyagi et al. [32] conducted a thorough analysis of the use of nanofluids in jet impingement/spray cooling, analyzing significant operational and design factors, along with different applications.

They highlighted critical factors for effective NF cooling, counting fluid properties, substrate characteristics, and other operational variables. Similarly, Mohammadpour et al. [33] conducted a comprehensive review of nano-jet cooling, examining different models of nanofluids modeling, such as single-phase and two-phase models and non-Newtonian fluid behavior. They analyzed both swirl-type impinging jets and conventional ones, noting that while single-phase non-Newtonian models resulted in higher HTR, they also required more pumping power. In their study, Modak et al. [34] conducted experimental analyses of CuO-water nano-jet's heat transfer rate characteristics on a hot square stainless steel foil surface. They utilized two different loading concentrations of CuO-water nanofluids. They observed a significant increase of about 90% in the Nusselt number (Nu) at the highest loading concentration. Besides that, there has been a growing interest in studying pulsating flow (PF) and its impact on heat transfer performance in recent years. Numerous experimental and numerical simulation studies have investigated the effects of various factors on HTR, such as pulsating amplitude, frequency, and Re number. These studies have demonstrated the potential of PF to significantly enhance HT in various applications [35]–[39]. The influence of PF and magnetic field on heat transfer rate inside a grooved channel filled with a hybrid nanofluid was numerically investigated by Lioua Kolsi et al. [40]. The findings showed that the Nu was elevated by 79.82% due to the amplitude of the pulsing flow. Abhijith M.S et al. [41] studied the effect of jet flow of a confined, incompressible jet colliding with several nanofluids, where the heat transfer rate increased by 60% and 25% using water-copper, water, and ammonia, respectively, compared to the basic fluid. Bin Sun et al. [42] studied the effect of traditional and vortex impact jet flow on different thermal surfaces and under different twisting conditions. The results obtained showed that thermal efficiency increases with increasing mass ratio, and that the heat transfer rate of vortex impact jets is higher than that of traditional impact jets.

A novel cooling method for solar systems and thermal management was recently suggested by Samah Maatoug et al. [43] used pulsating flow for several nano/hybrid fluids, where the Nu was improved by 63.5% using pulsating flow. The pulse amplitude of the flow and the slot number plays an essential role in the increase in the rate of heat.

A literature review has found that forced convection in a channel with the effect of sinusoidal elasticity on an obstacle and pulsating flow has not yet been reported. This unique configuration could be used in practical applications where flexible boundaries are present or where part of the obstacle can be made partially elastic to control flow and heat transfer characteristics. New insights into optimizing heat transfer and fluid flow in systems with flexible boundaries could be gained by exploring this novel approach to forced convection. This study proposes a new model for effective thermal management of a channel with sinusoidal elastic obstacles and pulsating multiple nano-jet impingement. The effects of pulse amplitude, sinusoidal elasticity, number of slots, nano/hybrid fluids, and Strouhal number on heat transfer rate will be investigated. The results of this research could be used to develop thermal applications and improve thermal management.

2. Mathematical formulation and modeling

2.1. Definition and formulation of the problem

The present study focuses on the analysis of the cooling of channels with sinusoidal elastic obstacles using a slot jet impinging system under pulsating flow (PF) conditions. The slot jet, with a confined width of IJ and the height of channels H , is shown schematically in Figure 1(a). As for the obstacles, their length represents 0.2 of the length of the channel, and their width is 0.02 of the height of the channel; Figure 1(b) shows the straight obstacles at ($t = 0$), and Figure 1(c) the sinusoidal obstacles at ($t \neq 0$). The channel was filled with a hybrid nanofluid (multi-wall carbon nanotube- Fe_3O_4) and a nanofluid consisting of nanoparticles of alumina Al_2O_3 in various forms (platelets, blades, cylinders, and bricks) and water as a basic fluid. In this study, the volume fractions for hybrid and Al_2O_3 nanofluid were 3%.

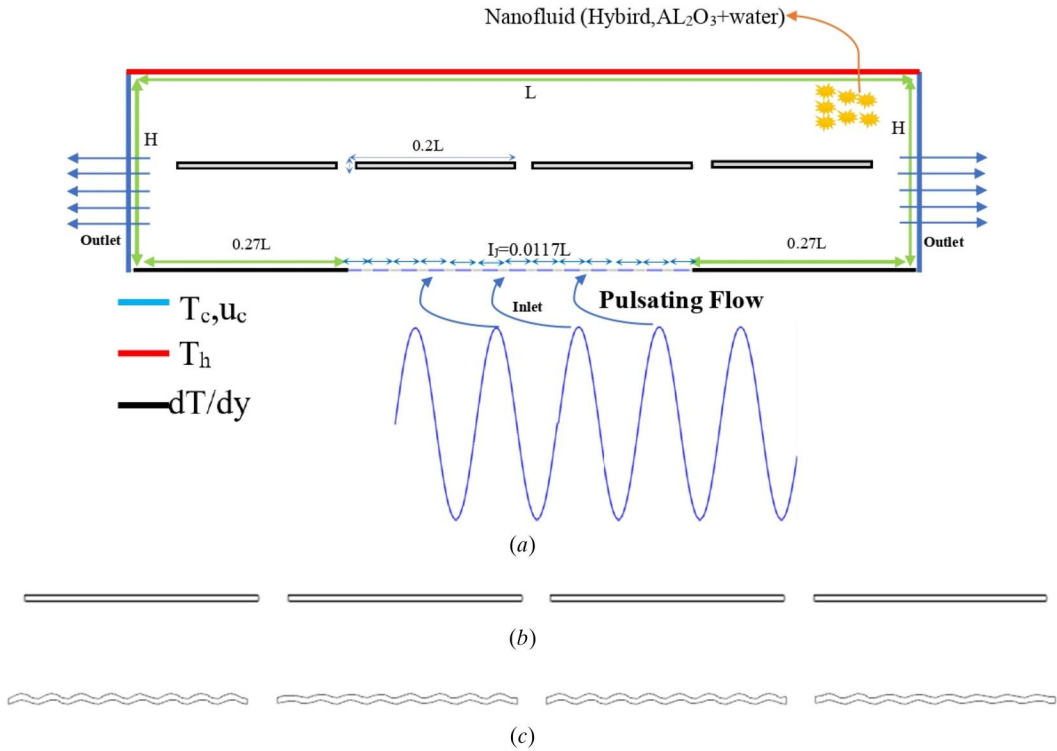


Figure 1. A schematic view of (a) channel with sinusoidal elastic obstacles and pulsating multiple nano-jet impingements, (b) straight obstacles at $t = 0$, and (c) sinusoidal obstacles at $t \neq 0$.

It should be noted that the sinusoidal elastic of the obstacles is entirely related to time. The cooling of the channel exposed to temperature from the top wall is achieved using pulsed flow. The coolant (nanofluid/hybrid) enters at T_c and at each jet velocity, the coolant pulsates according to the function $u_c = u_0(1 + A \sin(2\pi f t))$, where A and f represent the pulsating amplitude and frequency. This analysis considers an unsteady conjugate-type forced convective heat transfer regime. The flow is assumed to be laminar, two-dimensional, and transient.

The equations that govern two-dimensional transient laminar convection can be expressed in a dimensionless form by neglecting the effects of viscous dissipation, thermal conduction, and radiation [44].

$$\frac{\partial u}{\partial x} + \frac{\partial v}{\partial y} = 0 \quad (1)$$

$$\frac{\partial u}{\partial t} + u \frac{\partial u}{\partial x} + v \frac{\partial u}{\partial y} = -\frac{1}{\rho} \frac{\partial p}{\partial x} + \nu \left(\frac{\partial^2 u}{\partial x^2} + \frac{\partial^2 u}{\partial y^2} \right) \quad (2)$$

$$\frac{\partial v}{\partial t} + u \frac{\partial v}{\partial x} + v \frac{\partial v}{\partial y} = -\frac{1}{\rho} \frac{\partial p}{\partial y} + \nu \left(\frac{\partial^2 v}{\partial x^2} + \frac{\partial^2 v}{\partial y^2} \right) \quad (3)$$

$$\frac{\partial T}{\partial t} + u \frac{\partial T}{\partial x} + v \frac{\partial T}{\partial y} = \alpha \left(\frac{\partial^2 T}{\partial x^2} + \frac{\partial^2 T}{\partial y^2} \right) \quad (4)$$

where $\alpha = k/(\rho C_p)$

Table 1. Thermophysical properties of carbon nanotube-Fe₃O₄ hybrid nanofluid at various volume fractions and temperatures [45].

Volume fraction/%	T/°C	$\rho_{hnf}/kg.m^{-3}$	$k/Wm^{-1}K^{-1}$	$\mu/MP.s$	$C_p/J.Kg.K$
$\varphi = 0$ (base fluid)	20	998.5	0.602	0.79	4182
	40	992	0.631	0.54	4179
$\varphi = 0.1$	20	1002.34	0.6734	0.91	4182.66
	40	995.85	0.72	0.61	4179.66
$\varphi = 0.3$	20	1010.04	0.6856	1.01	4183.99
	40	1003.56	0.7656	0.76	4180.99

Table 2. Thermophysical properties of MWCNT and Fe₃O₄ nanoparticles [45].

Property	$\rho_{hnf}/kg.m^{-3}$	$k/Wm^{-1}K^{-1}$	$C_p/J.Kg.K$
Fe ₃ O ₄	5180	6	670
MWCNT	2100	3000	711

Table 3. Thermophysical properties of Al₂O₃-water nanofluid.

Property	$\rho_{hnf}/kg.m^{-3}$	$k/Wm^{-1}K^{-1}$	$C_p/J.Kg.K$
Water	998.5	0.602	4182
Al ₂ O ₃	3970	40	765

The Reynolds number (Re), Prandtl number (Pr), pressure coefficient (C_p), and Strouhal number (St) are significant non-dimensional numbers. These parameters are defined as follows:

$$Re = \frac{u_c D_h}{\nu_f}, Pr = \frac{\mu C_p}{k}, St = \frac{f D_h}{u_c}, \theta = \frac{T - T_c}{T_h - T_c}, C_p = \frac{P_{in} - P_{out}}{0.5 \rho u_c^2} \quad (5)$$

where $u_c, \nu_f, f, D_h, \theta$ the inlet velocity, kinematic viscosity, frequency, hydraulic diameter (characteristic length), and dimensionless temperature, respectively.

The boundary conditions considered for numerical simulation included the following items:

- At the inlet of the jet: $u = u_c, T = T_c$
- At the outlet: $\frac{\partial u}{\partial x} = \frac{\partial T}{\partial x}, \nu = 0$
- At the top wall: $T = T_h, \nu = u = 0$
- At sinusoidal elastic obstacles and the walls of the confined jet: $\frac{\partial T}{\partial n} = 0, \nu = u = 0$

2.2. Nanofluid thermophysical properties

When calculating the values of hybrid nanofluids' thermophysical characteristics, no single correlation can be employed. To investigate the characteristics of MWCNT-Fe₃O₄ hybrid nanofluids, this work uses the experimental data from Table 1. The thermophysical characteristics of nanoparticles made of MWCNT and Fe₃O₄ are shown in Table 2.

An Al₂O₃-water nanofluid was also used with four forms of nanoparticles (platelets, blades, cylinders, and bricks), as Table 3 shows the thermophysical properties of the fluid and the nanoparticles used:

For calculating the thermophysical properties of Al₂O₃-water nanofluids with four shapes of nanoparticles, the following equation was used:

$$\rho_{nf} = (1 - \varphi)\rho_f + \varphi\rho_s \quad (6)$$

$$(\rho C_p)_{nf} = (1 - \varphi)(\rho C_p)_f + \varphi(\rho C_p)_s \quad (7)$$

Table 4. Al₂O₃ nanoparticle constant values for various forms [46].

Shape	C _k	A ₁	A ₂
Platelets	2.61	37.1	612.6
Blades	2.74	14.6	123.3
Cylinders	3.95	13.5	904.4
Bricks	3.37	1.9	471.4

$$(\rho\beta)_{nf} = (1 - \varphi)(\rho\beta)_f + \varphi(\rho\beta)_s \quad (8)$$

The thermal conductivity and viscosity relations are stated as follows when considering the shape effect of nanoparticles [46]:

$$k_{nf} = k_{bf}(1 + C_k\varphi) \quad (9)$$

$$\mu_{nf} = \mu_{bf}(1 + A_1\varphi + A_2\varphi) \quad (10)$$

where Table 4 provides constants C_k, A₁, and A₂ for various shape of nanoparticle:

2.3. Nusselt number

The following equation is used to determine the local Nusselt number and average Nusselt number, which describes the nanofluid flow:

$$Nu_x = \frac{h_x \cdot D_h}{k} \quad (11)$$

$$Nu_m = \frac{1}{L} \int_0^L Nu_x dx \quad (12)$$

In the case of unsteady flow, the cycle average Nu can be defined for one period of pulsation (τ_p) as shown below:

$$Nu_a = \frac{1}{\tau_p} \int_0^{\tau_p} Nu_{m,t} dt \quad (13)$$

where the spatial average-time dependant portion of Nu is denoted by sub-index (m, t). To quantify heat transfer improvement (HTE) in both the pulsating flow and steady-state flow the HTE can be defined as follow:

$$HTE = \frac{Nu_{m,pulsating} - Nu_{m,steady}}{Nu_{m,steady}} \times 100 \quad (14)$$

2.4. Methodology of solving the problem and grid mesh examine

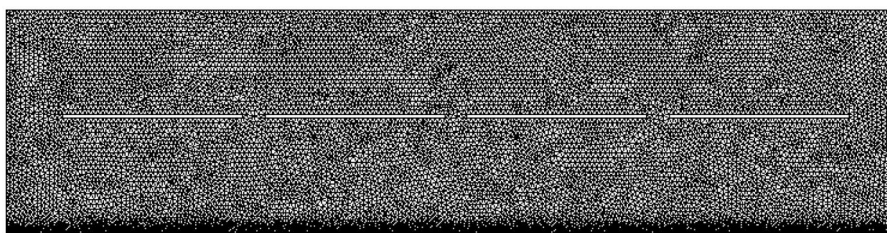
In order to assess the effectiveness of the proposed channel design in the presence of sinusoidal elastic obstacles, a numerical investigation was conducted using the ANSYS FLUENT computational fluid dynamics code [47]. The governing physical equations, including continuity, energy, and momentum, were solved using the finite volume method. The continuity and momentum equations were connected using the semi-implicit schemes for pressure-linked equations (SIMPLE). Spatial discretization of the convection terms was achieved through the use of the nonlinear upstream interpolation convection dynamics method, specifically the second-order upwind approach. An under-relaxation parameter of 1 is used for energy and quantity of movement, while a value of 0.3 is employed for pressure. The convergence criteria for the problem is set to 10⁻⁶.

Table 5. The remeshing criteria for present study.

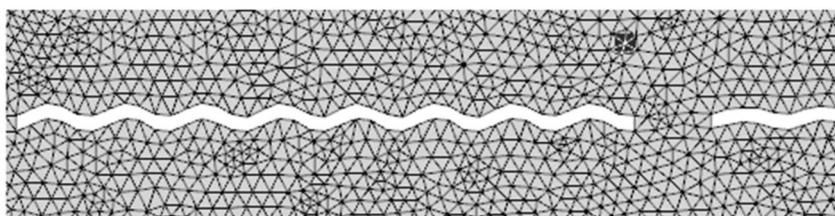
Minimum length scale (m)	5.05e – 05
Maximum length scale (m)	0.000624
Maximum cell skewness	0.7
Size remeshing interval	5

Table 6. The grid independence test for configuration.

No	$t = 0\text{ s}$		$t = 10\text{ s}$		T_m
	Node	Element	Node	Element	
G1	12598	23530	21226	40786	296.9511
G2	15001	28256	20390	39034	296.9536
G3	15460	29159	20071	38381	296.93
G4	17117	32424	18880	35950	296.9206
G5	17625	33418	17530	33238	296.9105



(a)



(b)

Figure 2. Grid distribution (a) channels with sinusoidal elastic obstacles (b) sinusoidal elastic obstacles.

Several elements of the grid mesh were tested for the investigation, including testing at the Reynolds number $Re = 350$, Strouhal number $St = 0.1$, and PLS-F amplitude ($A = 0.25$).

It should be highlighted that Re-meshing, which describes the process of creating new nodes that may be added to or deleted from the computational domain in order to alter the chosen mesh area, Mesh updating is often necessary when having dynamic geometries, fluid interactions with structures, or complex flow phenomena that require mesh adaptation during the simulation. The cells that need to be remeshed are determined by the remeshing criteria. The accessible standards are reported in Table 5.

It should be highlighted that Re-meshing, which describes the process of creating new nodes that may be added to or deleted from the computational domain in order to alter the chosen mesh area, was employed in the present work. Four scenarios with various element counts were taken into consideration in order to establish the grid mesh, as indicated in Table 6.

Figure 2 shows that the grid mesh G4 was calculated with 32424 triangular elements used in this study, where Figure 2(a) is channels with sinusoidal elastic obstacles and Figure 2(b) is the sinusoidal elastic obstacles.

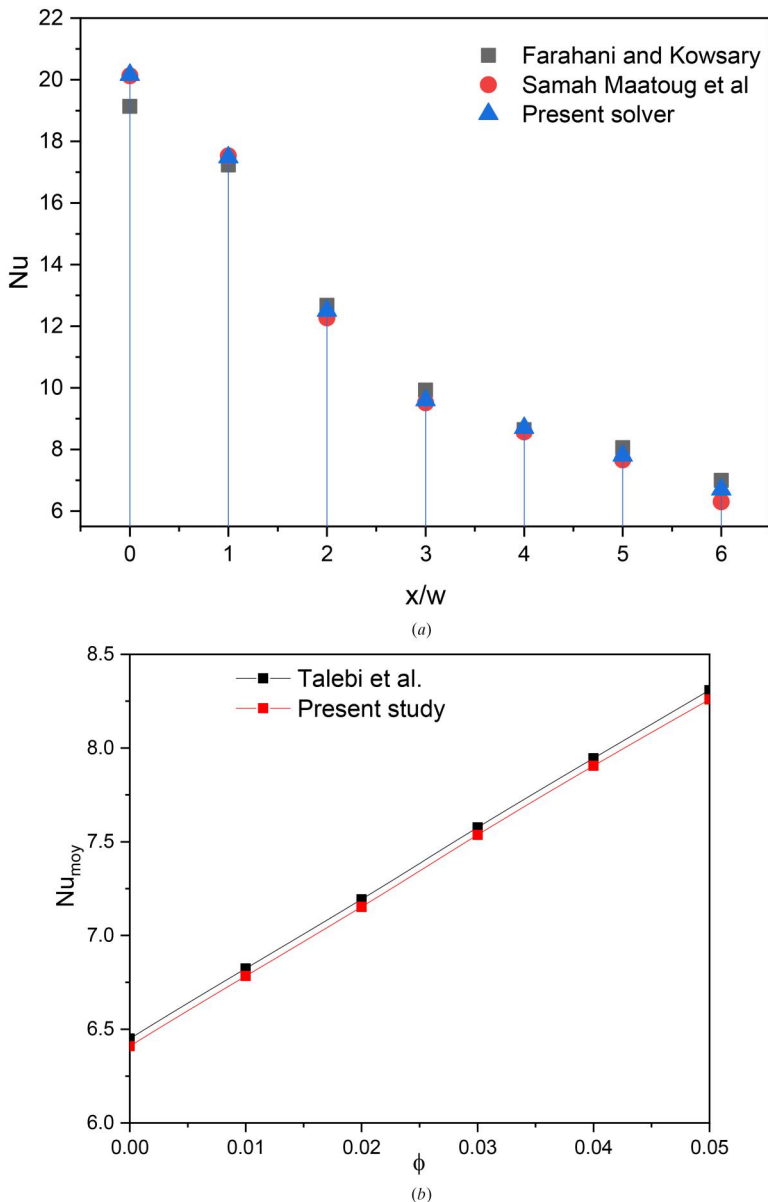


Figure 3. (a) The local Nusselt number of this study was compared to those of Farahani *et al.* [48] and Samah Maatoug *et al.* [43] at a Reynolds number of 900, $x/Dh = 4$, and a frequency of 80 Hz. (b) A comparison of the average Nusselt number between the current research and Talebi *et al.* [49].

2.5. Verification of code

To verify the validity of the proposed numerical study of the best heat dissipation methods. Numerical validation was carried out for two different studies. The first was according to the study conducted by Farahani *et al.* [48], where he conducted a numerical study of the effects of pulsating flow using numerical simulations, and the validity was verified by comparing the Nusselt number along the channel at a Reynolds number of 900, $x/Dh = 4$, and frequency 80 Hz.

According to Figure 3(a), it was found that the closeness between the studies was considered good because the error rate was equal to 0.3164%.

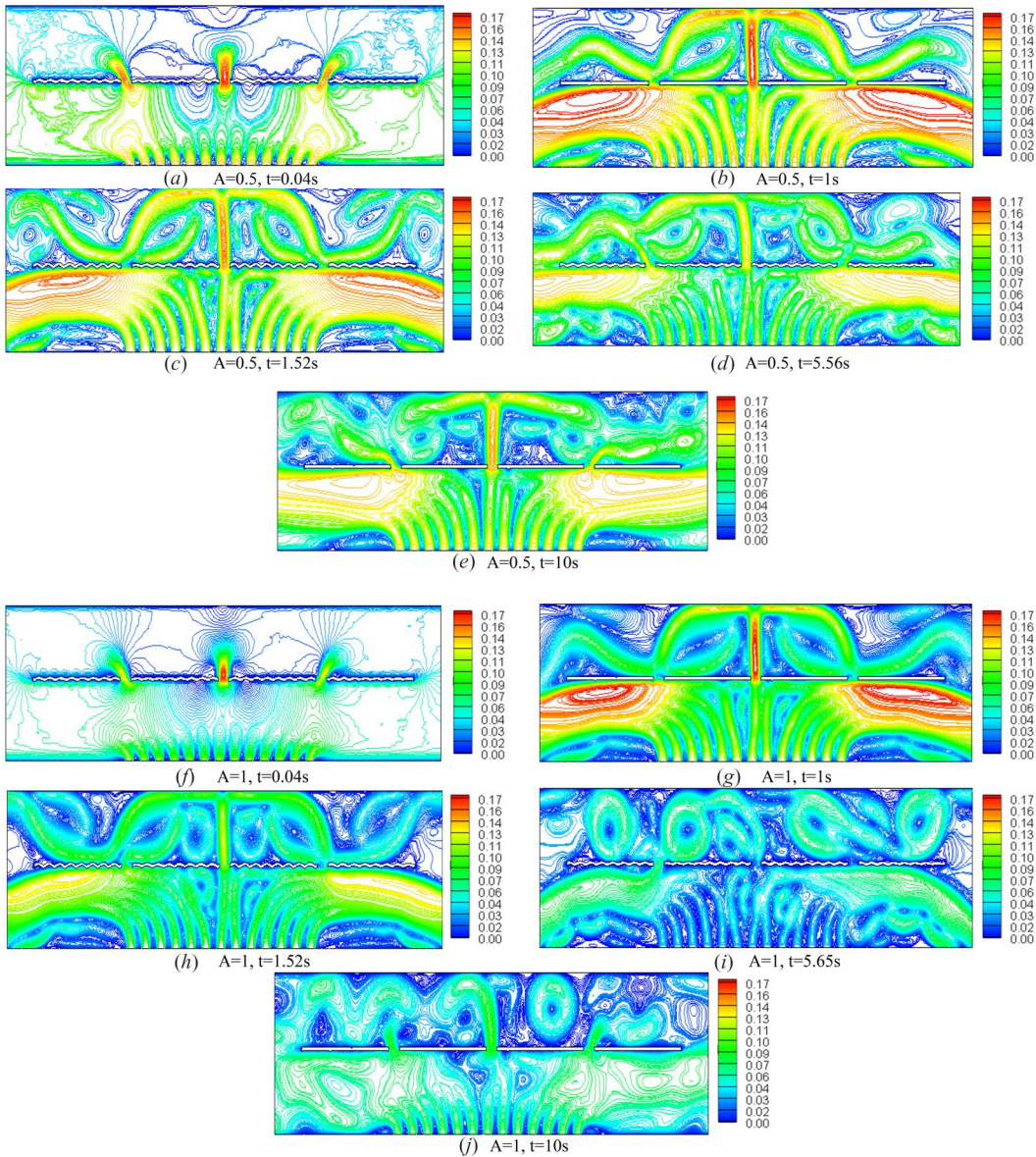


Figure 4. Variations in streamlines are depicted for different time instances of PLS-F for $a=0.5-1$ at $N_j = 13$, $St = 0.01$, $Re = 350$.

The second verification was according to a study conducted by F. Talebi *et al.* [49] where they studied the mixed convection inside a square cavity filled with the water-copper nanofluid, where **Figure 3(b)** shows the average Nusselt number at different volume fractions of the nanofluid at $Re = 100$, $Ra = 1.47 \times 10^5$. From the figure, we can say that the convergence between the results is very close, as the error rate reached -0.564% .

3. Results and discussions

To investigate the impact of sinusoidal elastic obstacles and Pulsating Nano-Jet Impingement on heat exchange, this study utilized Multi-wall carbon nanotube- Fe_3O_4 hybrid nanofluids and a

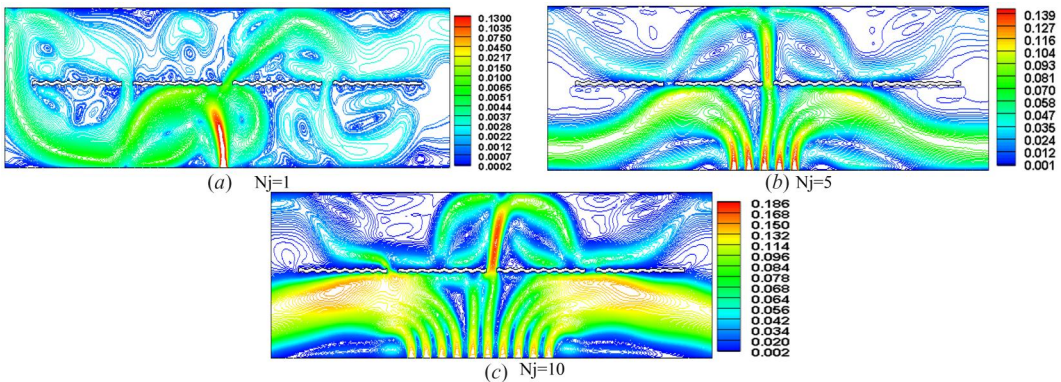


Figure 5. Variations in streamlines are depicted for different slot numbers of nano-jet impingement of PLS-F for $a=0.5$ at $t=5.56$ s, $St=0.1$, $Re=350$: (a) $Nj=1$, (b) $Nj=5$, (c) $Nj=10$.

nanofluid containing Al_2O_3 nanoparticles in various shapes (platelets, blades, cylinders, and bricks) with water as the base fluid. Results were obtained for multiple parameters, including a Reynolds number of $Re=350$, a Strouhal number range of ($St=0.01-1$), a Pulsating Amplitude range of ($A=0-1$), and a number of slots range of $Nj=(1-13)$, and reported accordingly. The initiation of flow pulsation effects occurs when the sinusoidal component of the velocity, which has an amplitude of A and a frequency of f , is superimposed, while in this study, it is considered the time step is $1/25$.

Figure 4(a-j) shows the streamline inside the channel for Multi-wall carbon nanotube- Fe_3O_4 hybrid nanofluids and for different time steps at a Strouhal number of $St=0.01$ and at an amplitude of $A=0.5-1$.

Figure 4(a-e) shows that the obstacles are flexible because the sinusoidal change appears in its original form. In addition, it appears that the pulsating flow creates vortices near the entrance, and the sinusoidal elastic obstacle also creates vortices due to the interaction between the fluid flow and the obstacle. Areas of high and low pressure are produced when the obstruction disrupts the fluid flow. Due to these high and low-pressure zones, the fluid is forced to flow obliquely and create vortices. The vortices are more prominent when a sinusoidal elastic obstruction is present due to the obstacle's flexibility. Due to the obstacle's flexibility, it may deform when subjected to fluid flow, which further disrupts the flow and intensifies the vortices. Vortices are also created by the obstructions' flexibility. With time and owing to the flexibility and pulsing flow, the vortices on the top side of the channel and walls improve, change in form, and become more numerous within the channel.

Figure 4(a-e) shows that the obstacles are flexible because the sinusoidal change appears in its original form. In addition, it appears that the pulsating flow creates vortices near the entrance, and the sinusoidal elastic obstacle also creates vortices due to the interaction between the fluid flow and the obstacle. Areas of high and low pressure are produced when the obstruction disrupts the fluid flow. Due to these high and low-pressure zones, the fluid is forced to flow obliquely and create vortices. Vortices can form in fluid flow across sinusoidal elastic obstacles due to the pressure gradient created by the sinusoidal shape. This pressure is strongest at the peaks and troughs of the sinusoidal shape, making vortices more likely to form there. Vortexes can interact with each other, with the walls of the channel, and with obstacles themselves.

The vortices are more prominent when a sinusoidal elastic obstruction is present due to the obstacle's flexibility. Due to the obstacle's flexibility, it may deform when subjected to fluid flow, which further disrupts the flow and intensifies the vortices. Vortices are also created by the obstructions' flexibility. These interactions can lead to complex and unpredictable vortex behavior, which can have a significant impact on fluid flow. With time and owing to the flexibility and

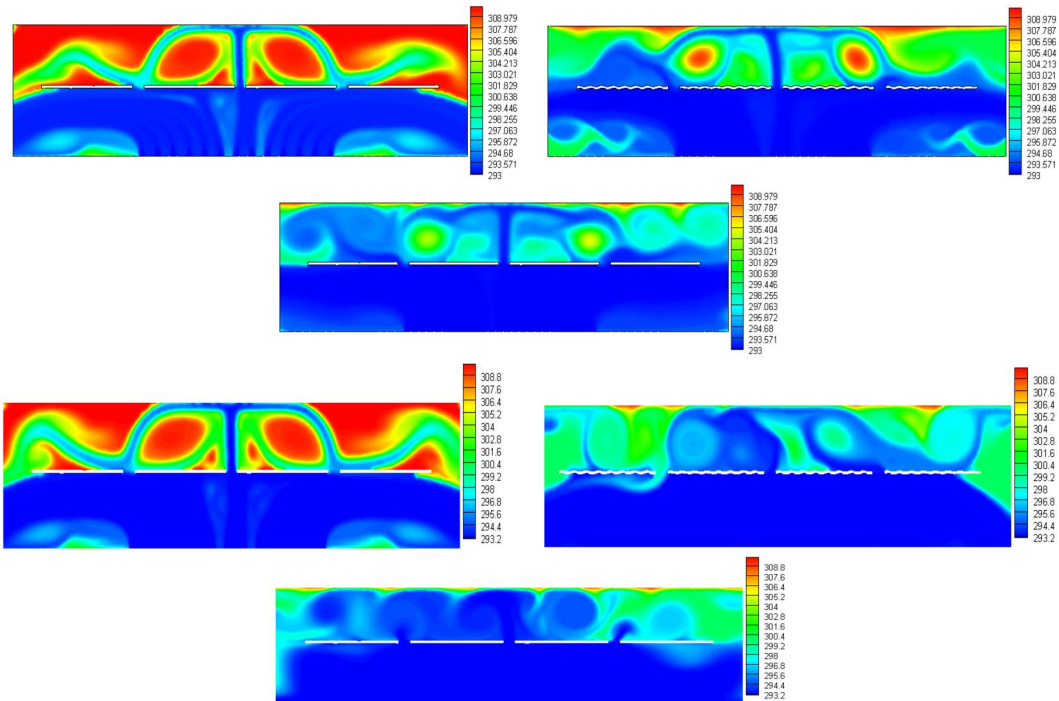


Figure 6. Variations in temperature profiles are depicted for different time instances of PLS-F for $a = 0.5-1$, $t = 1, 5.56, 10s$ at $N_j = 13$, $St = 0.01$, $Re = 350$.

pulsing flow, the vortices on the top side of the channel and walls improve these developments can lead to changes in the size and shape of the vortices, which may affect obstruction resistance and overall flow rate, and become more numerous within the channel.

Figure 4(i-j) shows that increasing the amplitude increases the number of vortices at the inlet and at the upper side of the channel. While increasing the amplitude increased the pulsating flow rate and thus led to an increase in turbulence in the fluid flow, the same applies to the pressure that increased at the inlet, which led to an increase in the shear force on the fluid, and this led to the movement of the fluid in different directions, and this led to the formation of vortices.

Figure 5(a-c) shows the streamline inside the channel for Multi-wall carbon nanotube-Fe₃O₄ hybrid nanofluids and for different slot numbers of nano-jet impingement $N_j = 1-10$. It can be seen that the variation in velocity within the channel increases with the number of slots. Increasing the inlets generates a flow pattern because the fluid enters the channel at varying rates, leading to noticeable differences in velocity, which creates an uneven flow distribution. In addition, the increase in the number of openings amplifies the turbulence in the flow. When streams of fluids emanating from different vents converge and interact, turbulent regions and eddies are formed. These turbulent regions exhibit diverse flow velocities and thus play a pivotal role in increasing the overall velocity variation within the channel.

Figure 6 shows the temperature profiles inside the channel for the number of inlets $N_j = 13$ for several periods of time and for a flow capacity of $A = 0.5-1$, as it is clear from the figure that the temperature the pulsating flow and the presence of sinusoidal elastic obstacles jointly affect the temperature profile within the fluid system, imparting complex thermodynamics to the environment. Pulsating flow introduces periodic changes in velocity and hence changes in convective heat transfer rates. During high-speed stages, convection-enhanced heat transfer occurs, which enhances the mixing of fluids at different temperatures. This results in a more uniform temperature distribution within the fluid. Conversely, during low-speed phases, heat transfer becomes less

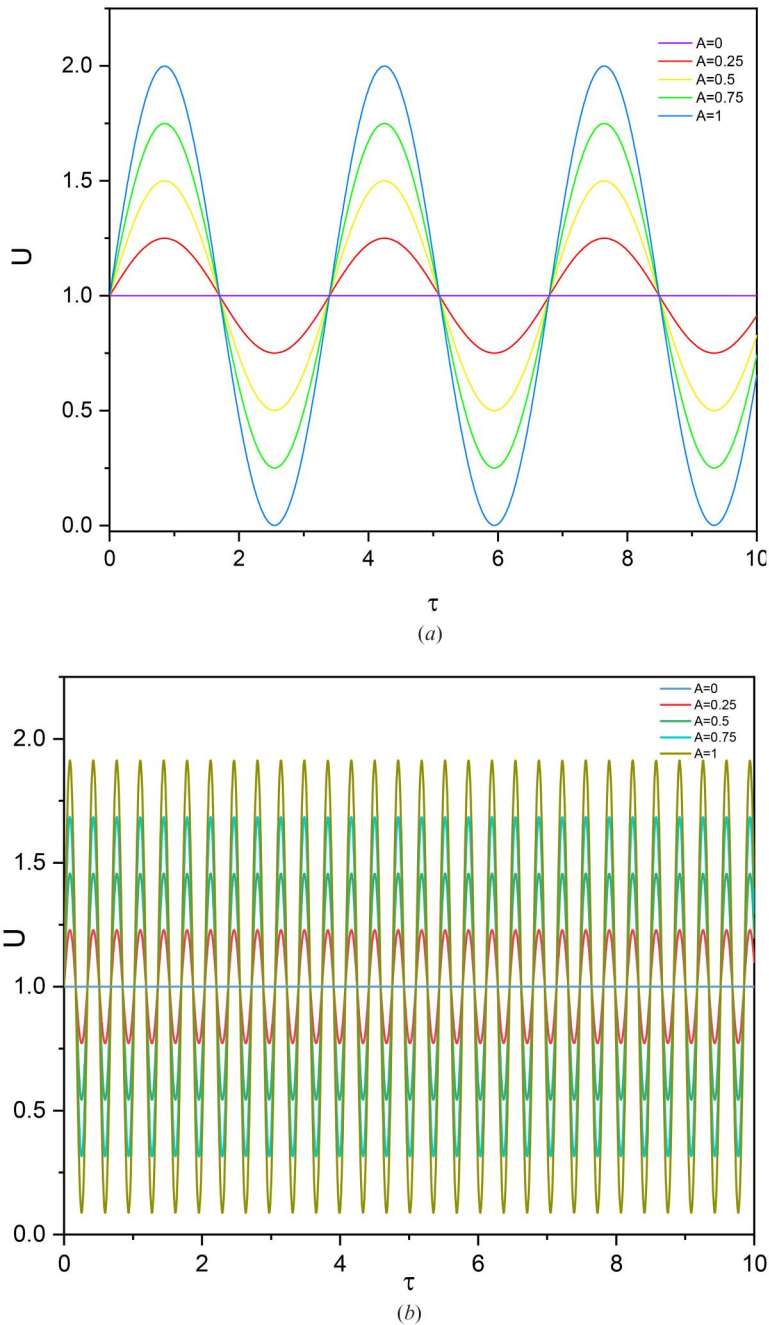


Figure 7. Variations in pulsating velocity are depicted for different time instances of PLS-F for different pulsating amplitude range $a = 0.25-1$ at $N_j = 13$, $Re = 350$ (a) $St = 0.01$, (b) $St = 0.1$, (c) $St = 1$.

efficient. Sinusoidal elastic barriers add another layer to this interaction. Deformation of these obstacles under the action of pulsating flow causes changes in flow patterns and pressure fields. This results in further temperature differences as the fluid interacts with the changing shape of the obstacle. Furthermore, heat transfer at the barrier–fluid interface is affected by deformations, which contributes to the overall temperature changes. The interaction between pulsating flow and

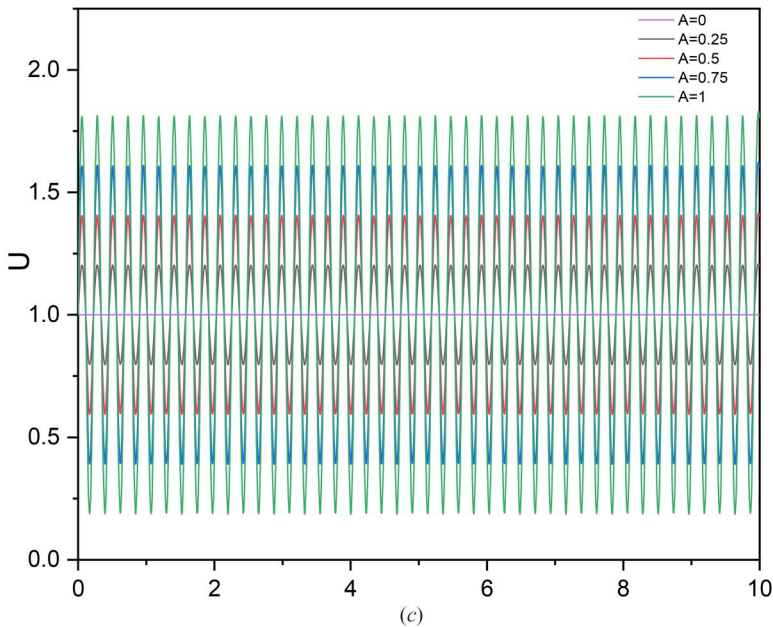


Figure 7. Continued.

sinusoidal elastic obstacles can lead to complex temperature oscillations and gradients, which ultimately affects the heat distribution in the system.

Figure 7 shows the variation in the Pulsating velocity the channel for Multi-wall carbon nanotube- Fe_3O_4 hybrid nanofluids of the number of slots $N_j = 13$, for different Strouhal number and pulse amplitudes, as it appears from Figures 6(a-c) that by increasing the Strouhal number from $St = 0.01$ to 1, the Pulse repetition frequency (PRF) increased. At Strouhal number $St = 0.01$, the average pulse velocity increased by 0.19%. By increasing the pulse amplitude $A = 0.25$ to 1, and at the Strouhal number $St = 1$, the average pulse velocity increased by 0.50%, as this increase is due to the increase in the frequency of the Pulsating flow. In general, it can be said that the Pulsating flow increased the average Inlet velocity at a pulse amplitude $A = 1$ of 0.67% compared to a constant flow.

Figure 8 shows the variation in dimensionless temperature for hybrid nanofluids and nanofluids with different particle shapes at $St = 0.1$ and $A = 0.5$. Figure 8(a) represents the dimensionless temperature of Multi-wall carbon nanotube- Fe_3O_4 hybrid nanofluid for several numbers of inlets $N_j = 1-13$, as it is clear from the figure. Still, the number of inlets affects the temperature, as the greater the number of inlets, the greater the ratio Cooling is better; the drop in temperature by increasing the number of inlets from 1 to 13 was 67.517%. Figure 8(b) also shows the variation in the dimensionless temperature of the Al_2O_3 -Water for many nanoparticle forms (blades, platelets, cylinders, and bricks). Bricks and blades have almost the same temperature contrast, but for platelets and cylinders, they have the best temperature contrast, as the percentage of temperature drop between platelets and bricks is 6.5009%.

Figure 9 shows the dimensionless temperature of two Strouhal number $St = 0.1-1$ at the numbers of slots $N_j = 13$, where Figure 9(a-b) shows the change in temperature in terms of time for several pulse amplitudes $A = 0.25-1$. The higher the pulse amplitude of the pulse flow, the faster the cooling process. At Strouhal number $St = 0.1$ and by increasing the pulse amplitude from $A = 0.25$ to 1, the channel cooling rate increased by 12.453%. When the Strouhal number was increased to $St = 1$, and the pulse amplitude was increased from $A = 0.25$ to 1, the channel cooling rate increased by 18.42%.

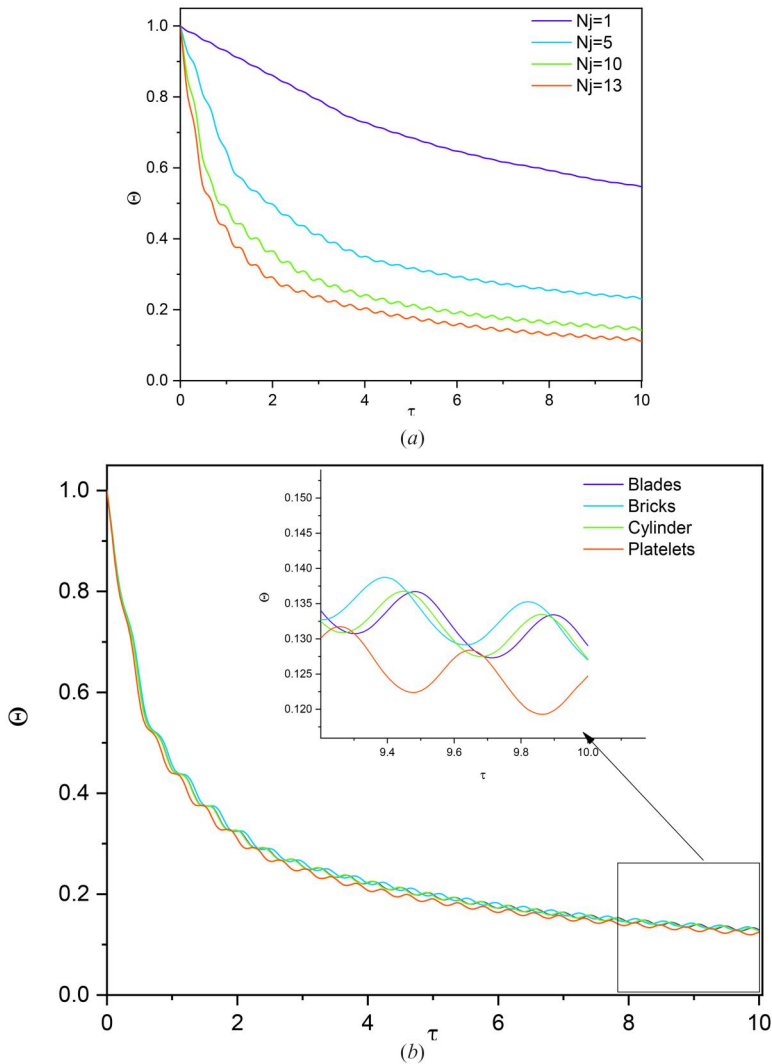


Figure 8. Variations in dimensionless temperature are depicted for different time instances of PLS-F at $N_j = 13$, $Re = 350$, $St = 0.1$, and $a = 0.5$, for (a) numbers of slots N_j , (b) different shapes of nanoparticles (platelets, blades, cylinders and bricks).

As mentioned previously, the current study studies the influence of sinusoidally elastic obstacles, where their effect on the local Nusselt number was studied, and this is illustrated in Figure 10 by using multi-wall carbon nanotube- Fe_3O_4 at $St = 0.1$, and $A = 0.5$, Figure 10(a) shows,

It depicts the hybrid nanofluid's local Nusselt number for various numbers of inlets when sinusoidal elastic obstacles are present, and it is obvious that the larger inlet number has a significant impact on the local Nusselt number. Due to an increase in the fluid's flow velocity *via* the surface, an increase in the input number raises the local Nusselt number. The fluid moves more quickly and comes into closer contact with the surface, increasing the rate of heat transfer.

As shown in Figure 10(b), the local Nusselt number of nanofluid in different shapes of nanoparticles (platelets, blades, cylinders and bricks) in the presence of sinusoidal elastic obstacles is $N_j = 13$, where it is clear that cylindrical and platelets nanoparticles have the highest rate of heat transfer.

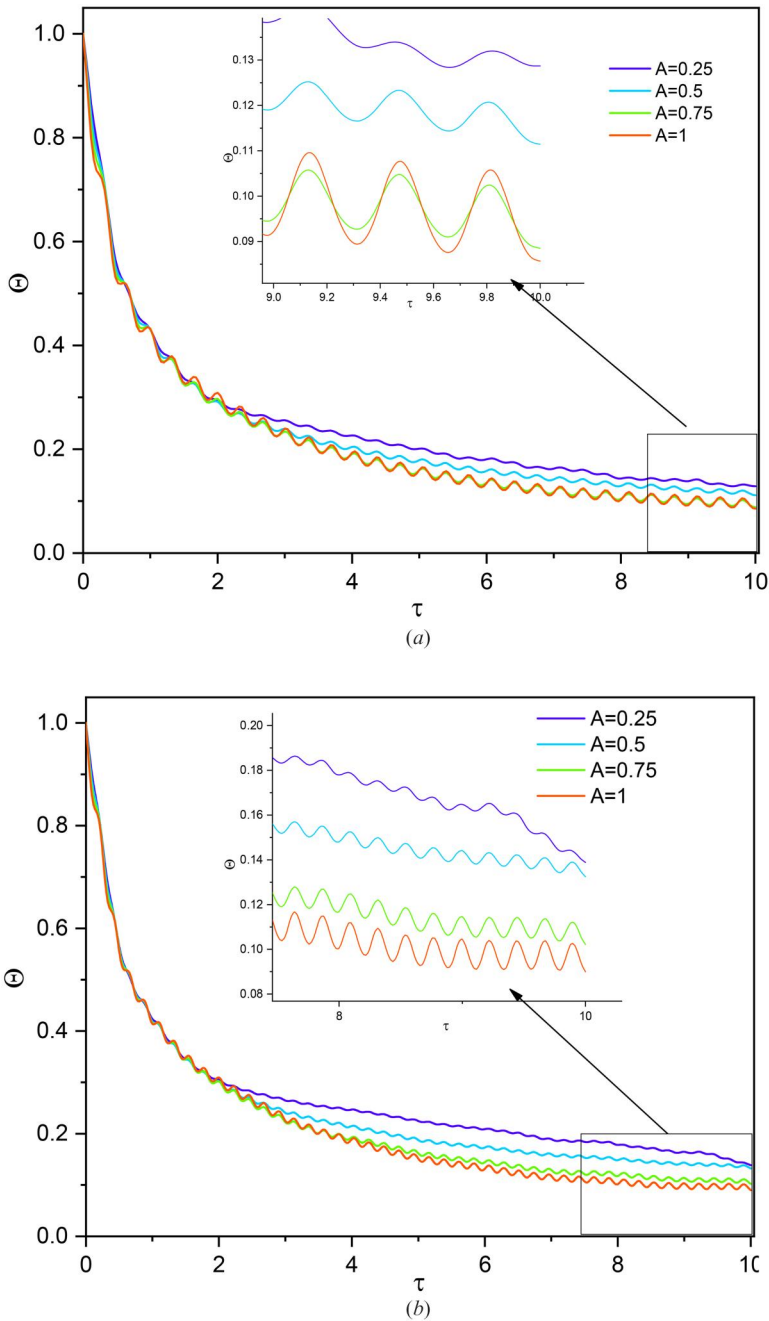
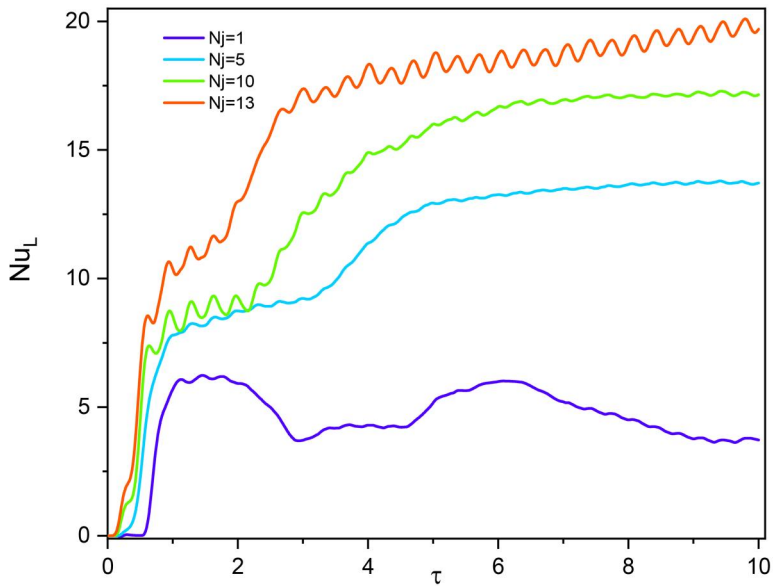
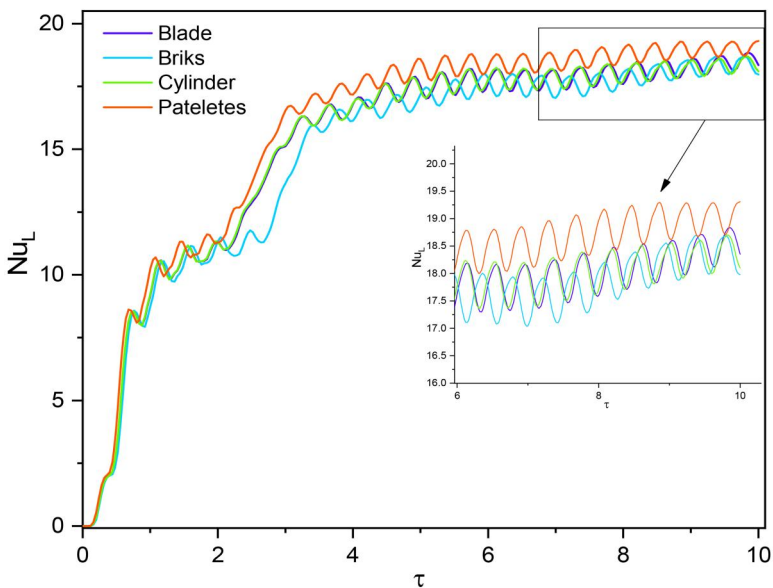


Figure 9. Variations in dimensionless temperature are depicted for different time instances of PLS-F at $N_j = 13$, $Re = 350$, for (a) $St = 0.1$, (b) $St = 1$.

Figure 11(a) compares the average Nusselt number (Nu_m) for different cases, starting from the channel without obstacles (CWO) and in the presence of fixed (COF) and sinusoidal elastic obstacles (COS), where the channel was filled with the base fluid in this case of comparison. Another comparison can be observed between the base fluid and the single and hybrid nanofluid with sinusoidal elastic obstacles, where the comparison was made At the $St = 0-0.01$, it can be



(a)



(b)

Figure 10. Variations in local Nusselt number are depicted for different time instances of PLS-F at $Re = 350$, $St = 0.1$, and $a = 0.5$, for (a) Numbers of slots N_j , (b) different shapes of Al_2O_3 -water nanofluid.

noted that the channel with sinusoidal flexible obstacles filled with a base fluid has improved the Nu_m , and this is due to sinusoidal movement of the obstacles, which in turn creates vortices inside the channel and the sinusoidal elastic obstacles helps to increase the surface area of the channel, which also increases the heat transfer rate, where the percentage of increase in the average Nusselt number is 8.344%. It can be noted that the use of single and hybrid nanofluids provided an average improvement of the Nusselt number by 1.822% and 6.53%, respectively. On the

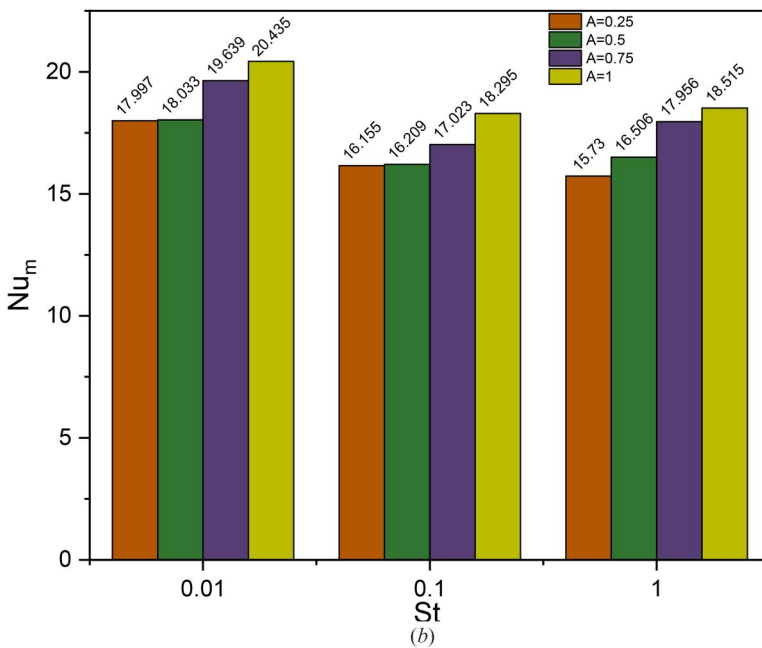
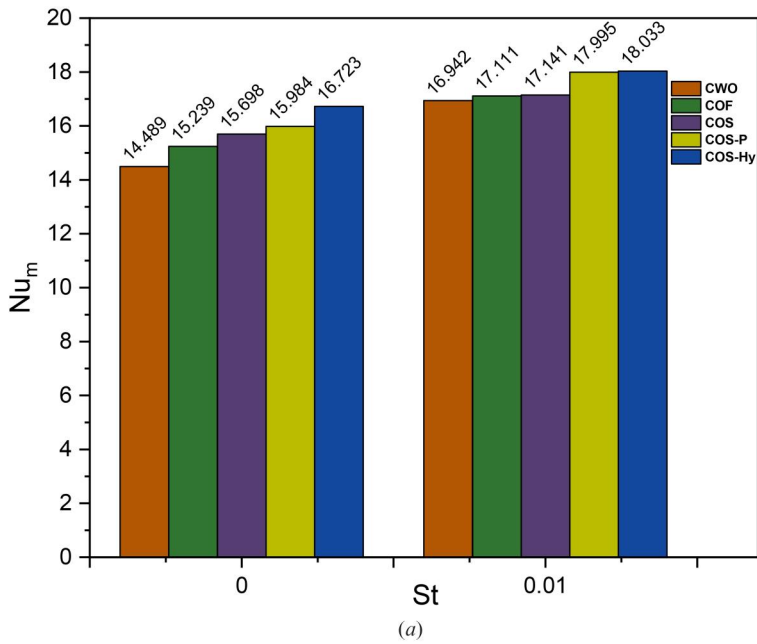


Figure 11. Variations in average Nusselt number (a) comparison of the Nu_m between multi case at $Re = 350$ and $a = 0-0.5$. (b) Nu_m for the different St and a for hybrid nanofluid. (c) Nu_m for different number of slots at $a = 0.5$. (d) Nu_m different shapes of nanoparticles for $St = 0.01-0.1$, and $a = 0.25-1$.

other hand, using pulsed flow within a sinusoidal elastic obstacle channel filled with a hybrid nanofluid improved by 24.383%.

Figure 11(b) represents the Nu_m for the different Strouhal numbers of the hybrid nanofluid and amplitude of the pulse flow. It also appears from the figure that the average Nusselt number

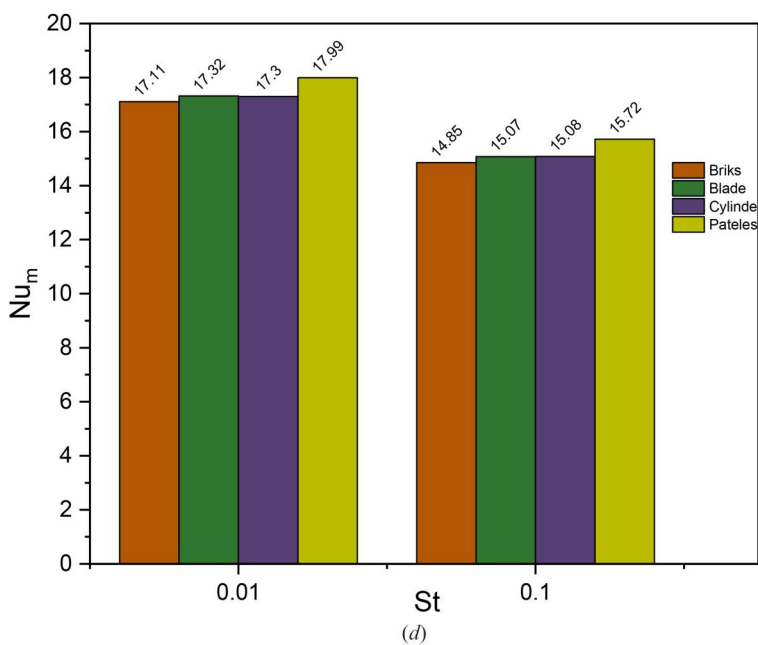
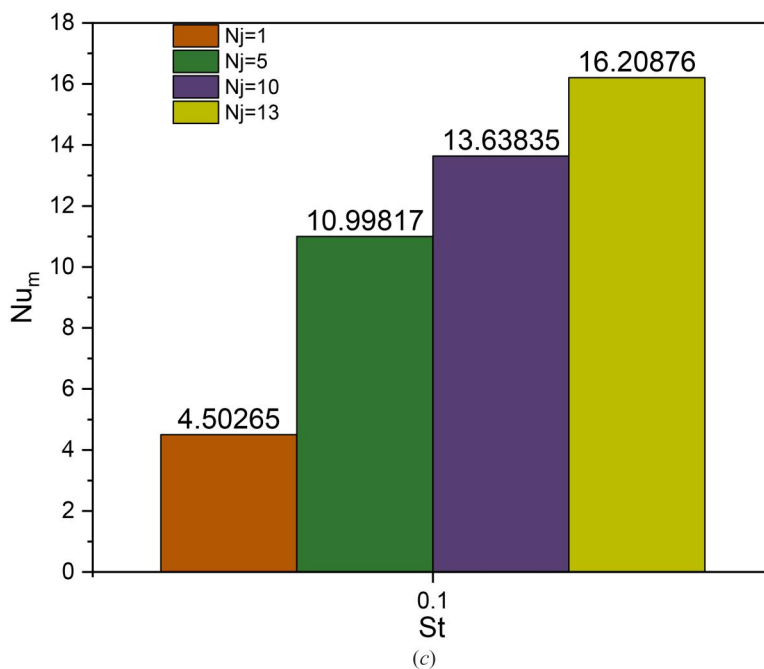


Figure 11. Continued.

decreases with an increase in the Strouhal numbers ($St = 0.01-1$) and increases with an increase in the amplitude of the pulse flow, as the increase reached ($A = 0.25 - 1$) by 13.5467%, 13.2467%, and 17.705%, respectively.

Figure 11(c) shows the Nu_m of the hybrid nanofluent at the Strouhal number $St = 0.1$ and the pulse amplitude $A = 0.5$ for the different number of slots, as it is clear from the figure that with

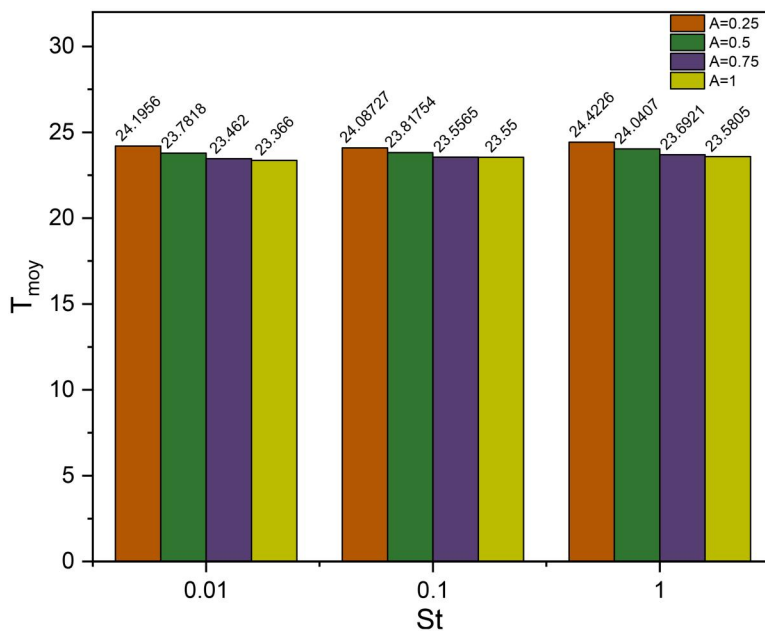


Figure 12. Variations in average temperature of hybrid nanofluent at $Re = 350$ $N_j = 13$, for pulse amplitude and different value of Strouhal number.

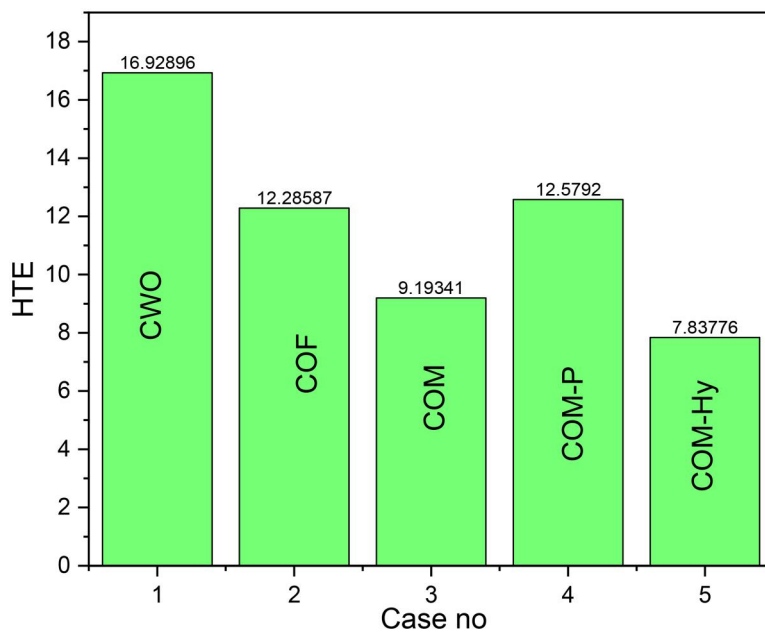


Figure 13. Percentage of enhancement in heat transfer by using pulsating nano-jet impingement for $St = 0-0.01$ and $\alpha = 0.5$.

increasing the number of slots, the average Nusselt number increases, and whereas, the percentage increase in the Nu_m when increasing the number of slots ($N_j = 1-13$) is 259.983%, and this is due to the increase in the flow inside the channel.

Figure 11(d) shows the average Nusselt number for different nanoparticle shapes of nanofluent Al_2O_3 -Water and for different Strouhal numbers at $A = 0.5$. Plate-shaped nanoparticles improved

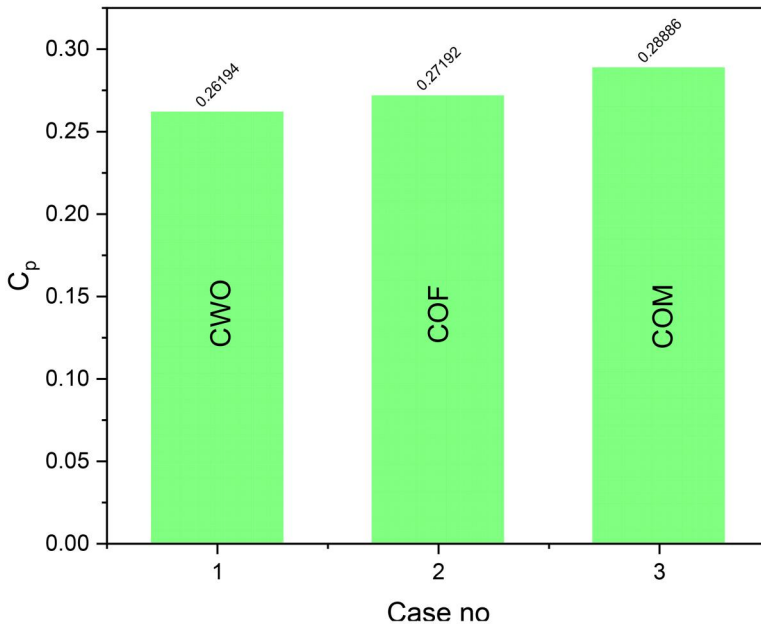


Figure 14. Pressure coefficient for various cases.

the Nu_m more than other particle types because particle shape is crucial to the heat transfer process; the average Nusselt number of plates improved by 5.18146% compared to bricks.

Figure 12 shows the average temperature of the different Strouhal number and the amplitude of the pulse flow, where it can be noted that with an increase in the pulse amplitude, the temperature decreases and thus the efficiency of thermal dissipation increases, as the best temperature levels were reported at $St = 1$, where the percentage of increase was 3.448%. While at $St = 0.1$, it amounted to 0.23% and at $St = 0.01$, it amounted to 3.42872%.

Figure 13 shows the percentage of enhancement in heat transfer using pulsating nano-jet impingement for the various studied issues, starting from the channel without elastic obstacles to using the hybrid nanofluid inside the channel with sinusoidal elastic obstacles, as it is clear from the figure that the use of pulsating nano-jet impingement has played an important role in the process of improving thermal performance, where the pulsating flow causes the fluid to be sheared more effectively, which breaks up the boundary layer and increases the heat transfer coefficient.

Figure 14 compares the pressure coefficient in the channel without obstacles to that with fixed obstacles and with sinusoidal elastic obstacles, showing that the pressure coefficient increases with fixed obstacles by 3.81767% due to the vortices caused by adding obstacles inside the channel and that it increases by 10.2772% with the latter due to the additional vortices caused by the movement of the obstacles.

Conclusion

This research paper has presented a new model for effective thermal management of a channel using elastic sinusoidal obstacles and pulsating multiple nano-jet impingement. The study employed various forms of alumina Al_2O_3 , such as platelets, blades, cylinders, and bricks, along with a hybrid nanofluid consisting of multi-wall carbon nanotube- Fe_3O_4 in a water base fluid. The mathematical equations governing the phenomenon were solved using the finite volume

method, the results were recorded for Reynolds numbers ($Re = 350$), Strouhal numbers ($St = 0.01-1$), pulse amplitude ($A = 0.25-1$), and the number of slots ($N_j = 1-13$).

In conclusion, the following key findings were observed:

The results showed that the use of pulsed flow affects the convection behavior inside the channel. The obstacles with sinusoidal elasticity formed vortices in the upper side of the channel. The sinusoidal elastic obstacles help to increase the surface area of the channel, which also increases the heat transfer rate. Using sinusoidal elastic obstacles improved the heat transfer rate by 8.344%. The Pulsating flow method resulted in a 24.383% increase in the rate of heat transfer. The heat transfer rate increased by 13.5467%, 13.2467%, and 17.705% when the Strouhal number (St) and pulse amplitude (A) were increased from $St = (0.01-1)$ and $A = (0.25-1)$, respectively. When the number of slots increased from ($N_j = 1-13$), the rate of heat transfer increased by an appropriate rate of 259.983%. The pressure coefficient increases by 3.81767% using fixed obstacles.

Based on the findings of this investigation, it seems that elastic sinusoidal obstacles might be used to enhance heat management. Investigating the impact of various elastic sinusoidal barriers' materials, forms, and dimensions on heat transmission would be interesting. Studying the impact of pulsing flow and elastic sinusoidal obstructions on the functionality of thermal management systems under various operating circumstances may also be effective.

Overall, the obtained results enable more efficient thermal management systems in numerous applications, giving valuable insight into using elastic sinusoidal barriers and pulsing flow.

Disclosure statement

No potential conflict of interest was reported by the author(s).

ORCID

Momen S.M. Saleh  <http://orcid.org/0000-0003-2605-4472>

Ali J. Chamkha  <http://orcid.org/0000-0002-8335-3121>

Yousra Boutera  <http://orcid.org/0000-0003-0048-7798>

References

- [1] A. J. Chamkha and E. Abu-Nada, "Mixed convection flow in single-and double-lid driven square cavities filled with water- Al_2O_3 nanofluid: effect of viscosity models," *Eur. J. Mech. B Fluids*, vol. 36, pp. 82-96, 2012. DOI: [10.1016/j.euromechflu.2012.03.005](https://doi.org/10.1016/j.euromechflu.2012.03.005).
- [2] F. Selimefendigil and H. F. Öztop, "Mixed convection of nanofluid filled cavity with oscillating lid under the influence of an inclined magnetic field," *J. Taiwan Inst. Chem. Eng.*, vol. 63, pp. 202-215, 2016. DOI: [10.1016/j.jtice.2016.03.003](https://doi.org/10.1016/j.jtice.2016.03.003).
- [3] B. Abbou, S. Mekroussi, H. Ameer and S. Kherris, "Effect of aspect ratio and nonuniform temperature on mixed convection in a double lid-driven cavity," *Numeri. Heat Transf. A Appl.*, vol. 83, no. 3, pp. 237-247, 2023. DOI: [10.1080/10407782.2022.2091365](https://doi.org/10.1080/10407782.2022.2091365).
- [4] E. Abu-Nada and A. J. Chamkha, "Mixed convection flow in a lid-driven inclined square enclosure filled with a nanofluid," *Eur. J. Mech. B Fluids*, vol. 29, no. 6, pp. 472-482, 2010. DOI: [10.1016/j.euromechflu.2010.06.008](https://doi.org/10.1016/j.euromechflu.2010.06.008).
- [5] R. Nasrin, M. A. Alim, and A. J. Chamkha, "Combined convection flow in triangular wavy chamber filled with water-CuO nanofluid: effect of viscosity models," *ICHMT.*, vol. 39, no. 8, pp. 1226-1236, 2012. DOI: [10.1016/j.icheatmasstransfer.2012.06.005](https://doi.org/10.1016/j.icheatmasstransfer.2012.06.005).
- [6] H. F. Öztop, "Combined convection heat transfer in a porous lid-driven enclosure due to heater with finite length," *ICHMT.*, vol. 33, no. 6, pp. 772-779, 2006. DOI: [10.1016/j.icheatmasstransfer.2006.02.003](https://doi.org/10.1016/j.icheatmasstransfer.2006.02.003).
- [7] F. Selimefendigil and H. F. Öztop, "Mixed convection in a partially heated triangular cavity filled with nanofluid having a partially flexible wall and internal heat generation," *J. Taiwan Inst. Chem. Eng.*, vol. 70, pp. 168-178, 2017. DOI: [10.1016/j.jtice.2016.10.038](https://doi.org/10.1016/j.jtice.2016.10.038).

- [8] A. Aghaei, H. Khorasanizadeh, G. Sheikhzadeh and M. Abbaszadeh, "Numerical study of magnetic field on mixed convection and entropy generation of nanofluid in a trapezoidal enclosure," *J. Magn. Magn. Mater.*, vol. 403, pp. 133–145, 2016. DOI: [10.1016/j.jmmm.2015.11.067](https://doi.org/10.1016/j.jmmm.2015.11.067).
- [9] T. Tayebi and A. J. Chamkha, "Entropy generation analysis during MHD natural convection flow of hybrid nanofluid in a square cavity containing a corrugated conducting block," *HFF*, vol. 30, no. 3, pp. 1115–1136, 2019. DOI: [10.1108/HFF-04-2019-0350](https://doi.org/10.1108/HFF-04-2019-0350).
- [10] M. S. M. Saleh, S. Mekroussi, S. Kherris, D. Zebbar and N. Belghar, "A numerical investigation of the effect of sinusoidal temperature on mixed convection flow in a cavity filled with a nanofluid with moving vertical walls," *Heat Trans*, vol. 52, no. 1, pp. 7–27, 2023. DOI: [10.1002/htj.22683](https://doi.org/10.1002/htj.22683).
- [11] M. S. M. Saleh, S. Mekroussi, S. Kherris, D. Zebbar, N. Belghar and A. J. Chamkha, "Effect of aspect ratios and sinusoidal temperature on heat exchange inside cavity filled with hybrid nanofluids," *J. Nanofluids*, vol. 12, no. 2, pp. 476–486, 2023. DOI: [10.1166/jon.2023.2002](https://doi.org/10.1166/jon.2023.2002).
- [12] M. S. M. Saleh, *et al.*, "Effect of rotating cylinder on nanofluid heat transfer in a bifurcating grooved channel equipped with porous layers," *Int. J. Mod. Phys. B*, vol. 37, no. 32, pp. 2350289, 2023. DOI: [10.1142/S0217979223502892](https://doi.org/10.1142/S0217979223502892).
- [13] M. S. M. Saleh, Y. Belloufi, Y. Boutera, A. J. Chamkha, A. Sahraoui and Q. Hroub, "A new design for a heat sink within a convex-parabolic microchannel filled with hybrid nanofluid for cooling Core I7 CPU," *J. Therm. Anal. Calorim.*, vol. 148, no. 20, pp. 11315–11324, 2023. DOI: [10.1007/s10973-023-12404-w](https://doi.org/10.1007/s10973-023-12404-w).
- [14] H. F. Oztop and I. Dagtekin, "Mixed convection in two-sided lid-driven differentially heated square cavity," *Int. J. Heat Mass Transf.*, vol. 47, no. 8–9, pp. 1761–1769, 2004. DOI: [10.1016/j.ijheatmasstransfer.2003.10.016](https://doi.org/10.1016/j.ijheatmasstransfer.2003.10.016).
- [15] A. R. M. Rosdzimin, S. M. Zuhairi and C. S. N. Azwadi, "Simulation of mixed convective heat transfer using lattice Boltzmann method," *Int. J. Automot. Mech. Eng.*, vol. 2, pp. 130–143, 2010. DOI: [10.1016/j.ijheatmasstransfer.2019.03.057](https://doi.org/10.1016/j.ijheatmasstransfer.2019.03.057).
- [16] Z. Boulahia, A. Wakif and R. Sehaqui, "Mixed convection heat transfer of Cu-water nanofluid in a lid driven square cavity with several heated triangular cylinders," *Int. J. Innov. Appl. Stud.*, vol. 2016, pp. 1–8, 2016. DOI: [10.1155/2016/8962091](https://doi.org/10.1155/2016/8962091).
- [17] Z. Boulahia, A. Wakif and R. Sehaqui, "Numerical investigation of mixed convection heat transfer of nanofluid in a lid driven square cavity with three triangular heating blocks," *IJCA*, vol. 143, no. 6, pp. 37–45, 2016. DOI: [10.5120/ijca2016910227](https://doi.org/10.5120/ijca2016910227).
- [18] B. Sharma, B. Kumar and R. N. Barman, "Numerical investigation of Cu-water nanofluid in a differentially heated square cavity with conducting solid square cylinder at center," *IJHT*, vol. 36, no. 2, pp. 714–722, 2018. DOI: [10.18280/ijht.360238](https://doi.org/10.18280/ijht.360238).
- [19] S. Hussain, M. Jamal and B. P. Geridonmez, "Impact of fins and inclined magnetic field in double lid-driven cavity with Cu–water nanofluid," *Int. J. Therm. Sci.*, vol. 161, pp. 106707, 2021. DOI: [10.1016/j.ijthermalsci.2020.106707](https://doi.org/10.1016/j.ijthermalsci.2020.106707).
- [20] F. Garoosi, L. Jahanshaloo, M. M. Rashidi, A. Badakhsh and M. E. Ali, "Numerical simulation of natural convection of the nanofluid in heat exchangers using a Buongiorno model," *Appl. Math Comput.*, vol. 254, pp. 183–203, 2015. DOI: [10.1016/j.amc.2014.12.116](https://doi.org/10.1016/j.amc.2014.12.116).
- [21] A. Ben-Nakhi and A. J. Chamkha, "Conjugate natural convection in a square enclosure with inclined thin fin of arbitrary length," *Int. J. Therm. Sci.*, vol. 46, no. 5, pp. 467–478, 2007. DOI: [10.1016/j.ijthermalsci.2006.07.008](https://doi.org/10.1016/j.ijthermalsci.2006.07.008).
- [22] N. Ben Cheikh, A. J. Chamkha and B. Ben Beya, "Effect of inclination on heat transfer and fluid flow in a finned enclosure filled with a dielectric liquid," *Numer. Heat Transf. A Appl.*, vol. 56, no. 3, pp. 286–300, 2009. DOI: [10.1080/10407780903163389](https://doi.org/10.1080/10407780903163389).
- [23] A. Ben-Nakhi and A. J. Chamkha, "Effect of length and inclination of a thin fin on natural convection in a square enclosure," *Numer. Heat Transf.*, vol. 50, no. 4, pp. 381–399, 2006. DOI: [10.1080/10407780600619907](https://doi.org/10.1080/10407780600619907).
- [24] A. Ben-Nakhi and A. J. Chamkha, "Conjugate natural convection around a finned pipe in a square enclosure with internal heat generation," *Int. J. Heat Mass Transf.*, vol. 50, no. 11–12, pp. 2260–2271, 2007. DOI: [10.1016/j.ijheatmasstransfer.2006.10.036](https://doi.org/10.1016/j.ijheatmasstransfer.2006.10.036).
- [25] A. Raisi and I. Arvin, "A numerical study of the effect of fluid-structure interaction on transient natural convection in an air-filled square cavity," *Int. J. Therm. Sci.*, vol. 128, pp. 1–14, 2018. DOI: [10.1016/j.ijthermalsci.2018.02.012](https://doi.org/10.1016/j.ijthermalsci.2018.02.012).
- [26] S. M. H. Zadeh, S. A. M. Mehryan, E. Izadpanahi and M. Ghalambaz, "Impacts of the flexibility of a thin heater plate on the natural convection heat transfer," *Int. J. Therm. Sci.*, vol. 145, pp. 106001, 2019. DOI: [10.1016/j.ijthermalsci.2019.106001](https://doi.org/10.1016/j.ijthermalsci.2019.106001).
- [27] A. I. Alsabery, M. A. Sheremet, M. Ghalambaz, A. J. Chamkha and I. Hashim, "Fluid-structure interaction in natural convection heat transfer in an oblique cavity with a flexible oscillating fin and partial heating," *Appl. Therm. Eng.*, vol. 145, pp. 80–97, 2018. DOI: [10.1016/j.applthermaleng.2018.09.039](https://doi.org/10.1016/j.applthermaleng.2018.09.039).

- [28] M. A. Ismael and H. F. Jasim, "Role of the fluid-structure interaction in mixed convection in a vented cavity," *Int. J. Mech. Sci.*, vol. 135, pp. 190–202, 2018. DOI: [10.1016/j.ijmecsci.2017.11.001](https://doi.org/10.1016/j.ijmecsci.2017.11.001).
- [29] M. Ghalambaz, E. Jamesahar, M. A. Ismael and A. J. Chamkha, "Fluid-structure interaction study of natural convection heat transfer over a flexible oscillating fin in a square cavity," *Int. J. Therm. Sci.*, vol. 111, pp. 256–273, 2017. DOI: [10.1016/j.ijthermalsci.2016.09.001](https://doi.org/10.1016/j.ijthermalsci.2016.09.001).
- [30] F. Selimefendigil, H. F. Oztop and A. J. Chamkha, "MHD mixed convection in a nanofluid filled vertical lid-driven cavity having a flexible fin attached to its upper wall," *J. Therm. Anal. Calorim.*, vol. 135, no. 1, pp. 325–340, 2019. DOI: [10.1007/s10973-018-7036-y](https://doi.org/10.1007/s10973-018-7036-y).
- [31] E. Jamesahar, M. Sabour, M. Shahabadi, S. A. M. Mehryan and M. Ghalambaz, "Mixed convection heat transfer by nanofluids in a cavity with two oscillating flexible fins: a fluid-structure interaction approach," *Appl. Math. Model.*, vol. 82, pp. 72–90, 2020. DOI: [10.1016/j.apm.2019.12.018](https://doi.org/10.1016/j.apm.2019.12.018).
- [32] P. K. Tyagi, R. Kumar and P. K. Mondal, "A review of the state-of-the-art nanofluid spray and jet impingement cooling," *Phys. Fluids*, vol. 32, no. 12, pp. 121301, 2020. DOI: [10.1063/5.0033503](https://doi.org/10.1063/5.0033503).
- [33] J. Mohammadpour and A. Lee, "Investigation of nanoparticle effects on jet impingement heat transfer: a review," *J. Mol. Liq.*, vol. 316, pp. 113819, 2020. DOI: [10.1016/j.molliq.2020.113819](https://doi.org/10.1016/j.molliq.2020.113819).
- [34] M. Modak, S. S. Chougule and S. K. Sahu, "An experimental investigation on heat transfer characteristics of hot surface by using CuO-water nanofluids in circular jet impingement cooling," *J. Heat Transf.*, vol. 140, no. 1, pp. 012401, 2018. DOI: [10.1115/1.4037396](https://doi.org/10.1115/1.4037396).
- [35] G. Xinxin, X. Haonan, L. Xueying and R. Jing, "Flow and heat transfer characteristics of Coriolis-utilization rotating rectangular smooth cooling U-channel," *Appl. Therm. Eng.*, vol. 211, pp. 118420, 2022. DOI: [10.1016/j.applthermaleng.2022.118420](https://doi.org/10.1016/j.applthermaleng.2022.118420).
- [36] S. Akcay, "Numerical analysis of heat transfer improvement for pulsating flow in a periodic corrugated channel with discrete V-type winglets," *ICHMT*, vol. 134, pp. 105991, 2022. DOI: [10.1016/j.icheatmasstransfer.2022.105991](https://doi.org/10.1016/j.icheatmasstransfer.2022.105991).
- [37] D. X. Jin, Y. P. Lee and D.-Y. Lee, "Effects of the pulsating flow agitation on the heat transfer in a triangular grooved channel," *Int. J. Heat Mass Transf.*, vol. 50, no. 15–16, pp. 3062–3071, 2007. DOI: [10.1016/j.ijheatmasstransfer.2006.12.001](https://doi.org/10.1016/j.ijheatmasstransfer.2006.12.001).
- [38] B. Yang, T. Gao, J. Gong and J. Li, "Numerical investigation on flow and heat transfer of pulsating flow in various ribbed channels," *Appl. Therm. Eng.*, vol. 145, pp. 576–589, 2018. DOI: [10.1016/j.applthermaleng.2018.09.041](https://doi.org/10.1016/j.applthermaleng.2018.09.041).
- [39] U. Akdag, S. Akcay and D. Demiral, "Heat transfer enhancement with laminar pulsating nanofluid flow in a wavy channel," *ICHMT*, vol. 59, pp. 17–23, 2014. DOI: [10.1016/j.icheatmasstransfer.2014.10.008](https://doi.org/10.1016/j.icheatmasstransfer.2014.10.008).
- [40] L. Kolsi, F. Selimefendigil, K. Ghachem, T. Alqahtani and S. Algarni, "Pulsating nanofluid flow in a wavy bifurcating channel under partially active uniform magnetic field effects," *ICHMT*, vol. 133, pp. 105938, 2022. DOI: [10.1016/j.icheatmasstransfer.2022.105938](https://doi.org/10.1016/j.icheatmasstransfer.2022.105938).
- [41] M. S. Abhijith and K. Venkatasubbaiah, "Numerical investigation of jet impingement flows with different nanofluids in a mini channel using Eulerian-Eulerian two-phase method," *Therm. Sci. Eng. Prog.*, vol. 19, pp. 100585, 2020. DOI: [10.1016/j.tsep.2020.100585](https://doi.org/10.1016/j.tsep.2020.100585).
- [42] B. Sun, Y. Zhang, D. Yang and H. Li, "Experimental study on heat transfer characteristics of hybrid nanofluid impinging jets," *Appl. Therm. Eng.*, vol. 151, pp. 556–566, 2019. DOI: [10.1016/j.applthermaleng.2019.01.111](https://doi.org/10.1016/j.applthermaleng.2019.01.111).
- [43] S. Maatoug, *et al.*, "Pulsating multiple nano-jet impingement cooling system design by using different nanofluids for photovoltaic (PV) thermal management," *Case Stud. Therm. Eng.*, vol. 41, pp. 102650, 2023. DOI: [10.1016/j.csite.2022.102650](https://doi.org/10.1016/j.csite.2022.102650).
- [44] M. K. Moraveji, R. M. Ardehali and A. Ijam, "CFD investigation of nanofluid effects (cooling performance and pressure drop) in mini-channel heat sink," *ICHMT*, vol. 40, pp. 58–66, 2013. DOI: [10.1016/j.icheatmasstransfer.2012.10.021](https://doi.org/10.1016/j.icheatmasstransfer.2012.10.021).
- [45] S. A. M. Mehryan, M. Izadi, Z. Namazian and A. J. Chamkha, "Natural convection of multi-walled carbon nanotube-Fe₃O₄/water magnetic hybrid nanofluid flowing in porous medium considering the impacts of magnetic field-dependent viscosity," *J. Therm. Anal. Calorim.*, vol. 138, no. 2, pp. 1541–1555, 2019. DOI: [10.1007/s10973-019-08164-1](https://doi.org/10.1007/s10973-019-08164-1).
- [46] E. V. Timofeeva, J. L. Routbort and D. Singh, "Particle shape effects on thermophysical properties of alumina nanofluids," *J. Appl. Phys.*, vol. 106, no. 1, pp. 14304, 2009. DOI: [10.1063/1.3155999](https://doi.org/10.1063/1.3155999).
- [47] U. D. F. Manual, *ANSYS FLUENT 12.0*, 2009.
- [48] S. D. Farahani and F. Kowsary, "Heat transfer from pulsating laminar impingement slot jet on a flat surface with inlet velocity: sinusoidal and square wave," *Heat Transf. Eng.*, vol. 39, no. 10, pp. 901–913, 2018. DOI: [10.1080/01457632.2017.1338868](https://doi.org/10.1080/01457632.2017.1338868).
- [49] F. Talebi, A. H. Mahmoudi and M. Shahi, "Numerical study of mixed convection flows in a square lid-driven cavity utilizing nanofluid," *ICHMT*, vol. 37, no. 1, pp. 79–90, 2010. DOI: [10.1016/j.icheatmasstransfer.2009.08.013](https://doi.org/10.1016/j.icheatmasstransfer.2009.08.013).